catalysts

MDPI

Article

The Role of Nitrate on the Sol-Gel Spread Self-Combustion Process and Its Effect on the NH_3-SCR Activity of Magnetic Iron-Based Catalyst

Xing Ning [1], Zhi-bo Xiong [1,2,*], Bin Yang [1,2], Wei Lu [1,2] and Shui-mu Wu [1,3]

1 School of Energy and Power Engineering, University of Shanghai for Science & Technology, Jungong Road #516, Shanghai 200093, China; nx_1210@126.com (X.N.); usst_yangbin@163.com (B.Y.); luweinora@163.com (W.L.); wsm8855@126.com (S.-m.W.)

2 Shanghai Key Laboratory of Multiphase Flow and Heat Transfer in Power Engineering, University of Shanghai for Science & Technology, Jungong Road #516, Shanghai 200093, China

3 SPIC Powder Plant Operation Technology (Beijing) Co., Ltd., Future Technology City, Beijing 102209, China

* Correspondence: xzb412@usst.edu.cn

Received: 25 February 2020; Accepted: 6 March 2020; Published: 10 March 2020

Abstract: Sol-gel spread self-combustion is the burning of the complexing agent in dried gel and the oxidant. Meanwhile, high temperature takes place during the combustion process, which is harmful to the pore structure of the catalyst. The nitrate from metal nitrate precursors as an oxidant could participate in the spread of the self-combustion process. Therefore, the influence of nitrate from metal nitrate on the spread self-combustion of an iron–cerium–tungsten citric acid gel and its catalytic performance of NO_x reduction were investigated by removing nitrate via the dissolution of washing co-precipitation with citric acid and re-introducing nitric acid into the former solution. It was found that the removal of nitrate contributes to enhancing the NH_3–SCR activity of the magnetic mixed oxide catalyst. The NO_x reduction efficiency was close to 100% for $Fe_{85}Ce_{10}W_5$–CP–CA at 250 °C while the highest was only 80% for the others. The results of thermal analysis demonstrate that the spread self-combustion process of citric acid dried gel is enhanced by re-introducing nitric acid into the citric acid dissolved solution when compared with the removal of nitrate. In addition, the removal of nitrate helps in the formation of γ-Fe_2O_3 crystallite in the catalyst, refining the particle size of the catalyst and increasing its pore volume. The removal of nitrate also contributes to the formation of Lewis acid sites and Brønsted acid sites on the surface of the catalyst compared with the re-introduction of nitric acid. The in situ diffuse reflectance infrared Fourier transform spectroscopy (DRIFTS) demonstrates that both Eley–Rideal (E–R) and Langmuir–Hinshelwood (L–H) mechanisms exist over $Fe_{85}Ce_{10}W_5$–CP–CA at 250 °C with E–R as its main mechanism.

Keywords: selective catalytic reduction of NO_x; sol-gel; the spread self-combustion method; nitrate; magnetic γ-Fe_2O_3

1. Introduction

Nitrogen oxide (NO_x) emitted from coal-fired power plants and automobile engines has a strong negative influence on the environment and human health [1–6]. Selective catalytic reduction of NO_x with NH_3 (NH_3–SCR) is well known as the best available control technology (BACT) to reduce nitrogen oxides due to its high efficiency [7,8]. Meanwhile, there exists some drawbacks such as high cost, high-temperature conversion of SO_2 to SO_3, the toxicity, and volatility of vanadium species for the commercial vanadium-based catalyst [9–16]. Due to the non-toxicity, low cost, environment, and the outstanding redox ability between Fe^{III} and Fe^{II}, a series of iron-based mixed oxide catalysts prepared through co-precipitation, sol-gel, and impregnation methods have been developed by many

researchers [17–20]. However, the sol-gel spread self-combustion method, also called low-temperature combustion synthesis (LCS), which takes advantage of organics (citric acid, glucose, urea, and so on) as reactants and nitrates from metal nitrates as oxidants, has been widely used to obtain nano-particles, ultrafine powders, and metal oxide catalysts [21–26]. In our precious studies, a novel Fe–Ce–W mixed oxide catalyst synthesized via the citric acid sol-gel spread self-combustion method exhibited high catalytic activity of NO_x reduction with high-dispersive γ-Fe_2O_3 crystallite formed in it [27]. However, a large amount of heat is released during the spread self-combustion of the citric acid dried gel, and brings about a high temperature that acts on the obtained composite oxide catalyst, which might destroy the physical structure of catalyst, thereby influencing its catalytic performance of NO_x reduction even though the duration of high temperature is short. Previous research has demonstrated that the amount of complexing agent as the fuel participated in the spread self-combustion of the dried gel, and affected the rapid oxidation of Fe^{II} to Fe^{III} [28]. Meanwhile, the oxygen from the surrounding air as an oxidant showed an enhancement effect on the spread self-combustion process of dried gel, which affected the structure properties of the obtained powder [29]. The nitrate from metal nitrate precursors as another oxidant could also participate in the spread self-combustion of dried gel. Therefore, it is necessary to investigate the influence of nitrate on the spread self-combustion of dried gel, especially its effect on the NH_3–SCR activity over the above magnetic iron–cerium–tungsten mixed oxide catalyst.

Herein, in the present work, two kinds of magnetic iron–cerium–tungsten mixed oxide catalysts were synthesized via the spread self-combustion of citric acid gel by removing nitrate through the dissolution of washing co-precipitation with citric acid, and re-introducing nitric acid into the former citric acid dissolved solution, respectively. Thermo-gravimetric analysis (TG-DTG-DSC) was used to study the influence of nitrate on the combustion of citric acid gel. In addition, x-ray diffraction (XRD), N_2-adsorption–desorption, x-ray photoelectron spectroscopy (XPS), temperature-programmed reduction (H_2-TPR), temperature-programmed desorption (NH_3-TPD), and scanning electron microscope (SEM) were eventually used to characterize the physical structural and chemical properties of the catalyst.

2. Results and Discussion

2.1. NH_3–SCR Activity

As can be observed from Figure 1, magnetic $Fe_{85}Ce_{10}W_5$–CP–CA synthesized through the spread self-combustion of the citric acid dried gel without the nitrate from the metal nitrate precursors exhibited excellent catalytic performance of NO_x reduction at 150~400 °C, and more than 90% of NO_x reduction was achieved at 225~400 °C and over, under a gaseous hourly space velocity (GHSV) of 60,000/h. Meanwhile, the re-introduction of nitric acid into the citric acid dissolved solution decreased the NH_3–SCR activity of $Fe_{85}Ce_{10}W_5$–CP–CA, and the enhancement of nitrate ions from 0.5 to 2.0 further decreased its catalytic performance. This demonstrates that the nitrate brought from the precursors of metal nitrate shows an inhibition on the NH_3–SCR activity of the magnetic $Fe_{85}Ce_{10}W_5$ catalyst prepared through the spread self-combustion of citric acid gel. As shown in Table 1, the NO_x conversion over per gram of $Fe_{85}Ce_{10}W_5$–CP–CA at low temperature (125~200 °C) in one hour was still higher than those of $Fe_{85}Ce_{10}W_5$–CP–CA($NA_{1.0}$), although the bulk density of $Fe_{85}Ce_{10}W_5$–CP–CA was 0.7124 g/mL, which was higher than that of $Fe_{85}Ce_{10}W_5$–CP–CA($NA_{1.0}$). Apparently, the re-introduction of nitric acid could participate in the spread self-combustion of citric acid dried gel, thereby decreasing the bulk density of $Fe_{85}Ce_{10}W_5$–CP–CA. Therefore, the nitrate brought from the metal nitrate precursors shows an important role in the spread self-combustion of citric acid gel, thus affecting the physical structure and the redox properties of magnetic iron–cerium–tungsten mixed oxide catalyst. Herein, TG-DTG-DSC was used to investigate the combustion of the critic acid dried gels of $Fe_{85}Ce_{10}W_5$–CP–CA and $Fe_{85}Ce_{10}W_5$–CP–CA($NA_{1.0}$).

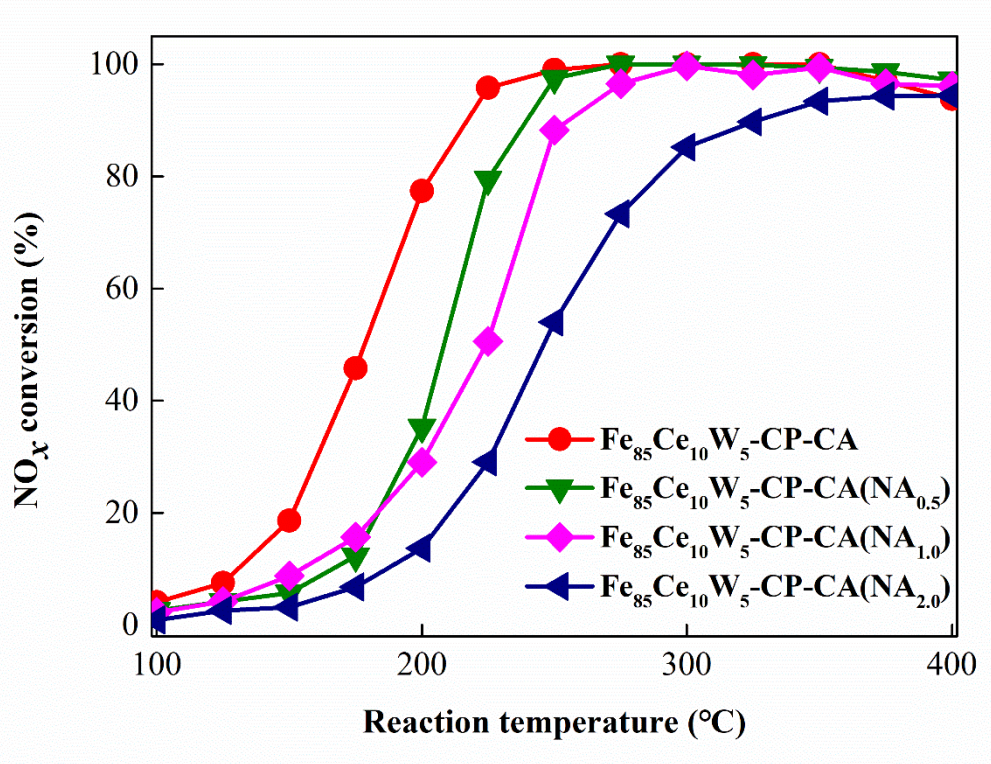

Figure 1. The NO_x conversion over the catalyst. Reaction conditions: [NO] = [NH_3] = 1000 ppm, [O_2] = 3.0 vol.% and 2000 mL/min of total flow rate. A total of 2 mL of catalyst with a gas hourly space velocity (GHSV) of 60,000/h.

Table 1. The NO_x conversion over per gram of catalysts under a gas hourly space velocity (GHSV) of 60,000/h.

Samples	NO_x Conversion (mg/(g·h))			
	125 °C	150 °C	175 °C	200 °C
$Fe_{85}Ce_{10}W_5$–CP–CA	8.5	21.0	51.6	87.3
$Fe_{85}Ce_{10}W_5$–CP–CA($NA_{1.0}$)	7.4	15.4	27.2	50.4

2.2. Thermo-Gravimetric Analysis (TG-DTG-DSC)

Thermal analysis was carried out to investigate the relationship between the weight loss of the catalyst and temperature. The thermo-gravimetric (TG), differential thermo-gravimetric (DTG), and differential scanning calorimetry (DSC) traces of the $Fe_{85}Ce_{10}W_5$–CP–CA and $Fe_{85}Ce_{10}W_5$–CP–CA($NA_{1.0}$) citric acid gels were tested and the results are shown in Figure 2. The gel of $Fe_{85}Ce_{10}W_5$–CP–CA($NA_{1.0}$) illustrates about 20% weight loss before approximately 140 °C, and a larger exothermic peak can be clearly observed from its DSC, which is mainly attributed to the decomposition of nitrate. However, the gel of $Fe_{85}Ce_{10}W_5$–CP–CA shows two steps weight loss compared to the three steps weight loss of $Fe_{85}Ce_{10}W_5$–CP–CA($NA_{1.0}$) gel. During the ignition, the gel of $Fe_{85}Ce_{10}W_5$–CP–CA($NA_{1.0}$) presents a sharply spread self-combustion at about 140 °C with a large quantity of reddish brown gas released due to the decomposition of nitrate. Meanwhile, there exists an exothermic peak at 110~160 °C for $Fe_{85}Ce_{10}W_5$–CP–CA($NA_{1.0}$) gel, or not an endothermic peak. This indicates that there exists a certain burning of citric acid at 110~160 °C, and this also enhances the main burning temperature of dried gel compared with that of $Fe_{85}Ce_{10}W_5$–CP–CA with a major mass loss about 37% at 160~220 °C. Therefore, the presence of NO_3^- helps with the burning or/and decomposing of the citric acid dried gel [30]. Finally, the exothermic peak at 240~350 °C with a smaller weight loss could be considered as the gradual decomposition of citrates (ferric citrate, etc.) for these two

dried gels. Meanwhile, the decomposition temperature of the gradual citrates for $Fe_{85}Ce_{10}W_5$–CP–CA is lower than those of $Fe_{85}Ce_{10}W_5$–CP–CA($NA_{1.0}$). Thus, it can be concluded that the existence of nitrate could enhance the spread self-combustion of citric acid gel, which affects the physical structure and redox properties of magnetic iron–cerium–tungsten mixed oxide catalyst, thereby influencing its low-temperature NH_3–SCR activity.

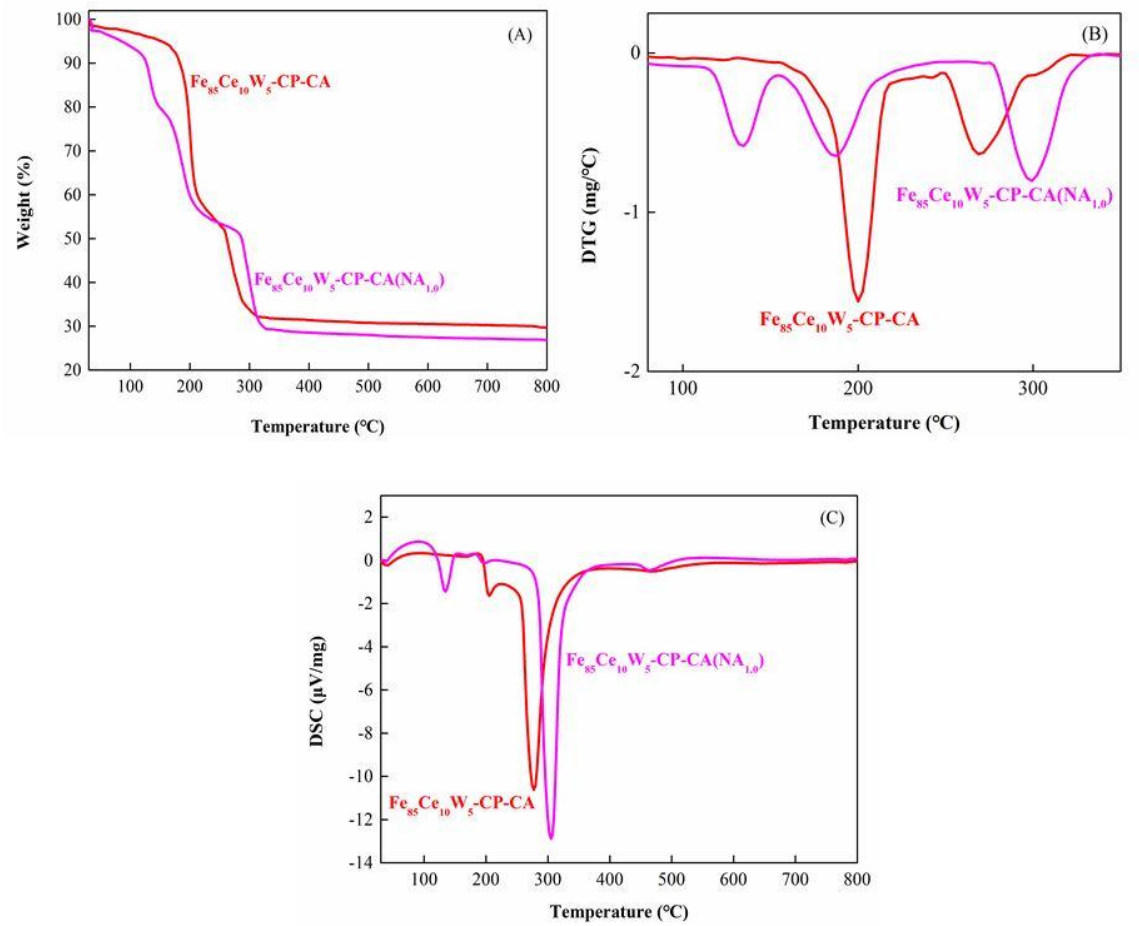

Figure 2. Thermal analysis curves of the precursor mixtures of Fe85Ce10W5–CP–CA and Fe85Ce10W5–CP–CA(NA1.0) recorded under an air atmosphere. (**A**) thermo-gravimetric (TG), (**B**) differential thermo-gravimetric (DTG), and (**C**) differential scanning calorimetry (DSC).

2.3. Structural Properties

2.3.1. X-Ray Diffraction

The X-ray diffraction patterns of $Fe_{85}Ce_{10}W_5$–CP–CA and $Fe_{85}Ce_{10}W_5$–CP–CA($NA_{1.0}$) were measured and the results are shown in Figure 3. It can be noted that there exists some obvious sharp diffraction peaks at 2θ = 30.2°, 35.6°, 43.3°, 53.7°, 57.4°, 62.7° in the samples, which are attributed to γ-Fe_2O_3 crystallite (#25-1402), and the diffraction peak at 2θ = 28.9° could be assigned to CeO_2 crystallite (#43-1002), according to the Joint Committee on Powder Diffraction Standards (JCPDS). This indicates that γ-Fe_2O_3 and CeO_2 are the main crystallites of magnetic Fe–Ce–W mixed oxide catalysts [19,31]. Meanwhile, the intensity of diffraction peaks attributed to the γ-Fe_2O_3 crystallite in $Fe_{85}Ce_{10}W_5$–CP–CA is stronger than that of $Fe_{85}Ce_{10}W_5$–CP–CA($NA_{1.0}$). Therefore, the removal of nitrate promotes the formation of γ-Fe_2O_3 crystallite, which is usually thought to be an important active specie for NH_3–SCR reaction [27]. The re-introduction of nitrate also weakens the crystallization of CeO_2 in $Fe_{85}Ce_{10}W_5$–CP–CA. Meanwhile, the average γ-Fe_2O_3 crystallite sizes of $Fe_{85}Ce_{10}W_5$–CP–CA

and $Fe_{85}Ce_{10}W_5$–CP-CA($NA_{1.0}$) as calculated according to the Scherrer equation were 13.0 and 14.4 nm, respectively. Therefore, the re-introduction of nitrate causes a large amount of combustion heat to be released and results in a high temperature, thereby enlarging the particle size of $Fe_{85}Ce_{10}W_5$–CP–CA. Then, the removal of nitrate helps in the formation of dispersive γ-Fe_2O_3 crystallites during the spread self-combustion of citric acid gel and restrains the inter-particle agglomeration and growth of the magnetic iron–cerium–tungsten mixed oxide catalyst.

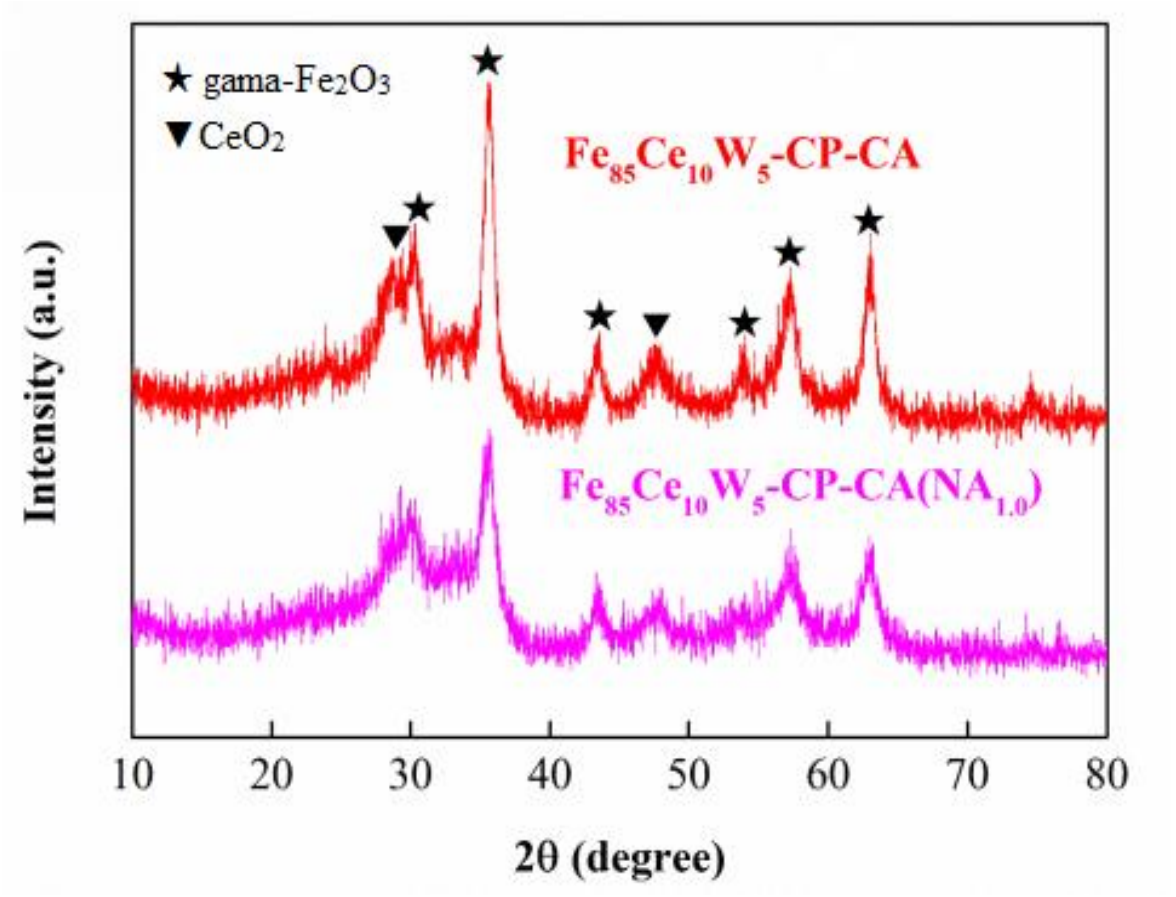

Figure 3. The x-ray diffraction (XRD) spectra of $Fe_{85}Ce_{10}W_5$–CP–CA and $Fe_{85}Ce_{10}W_5$–CP–CA($NA_{1.0}$). (★ gama-Fe_2O_3 25-1402, ▼ CeO_2 43-1002).

2.3.2. Scanning Electron Microscopy (SEM)

Scanning electron microscopy (SEM) is a useful technique to study the surface morphology, shape, and macroscopic particle size of the catalyst. Typical SEM pictures of $Fe_{85}Ce_{10}W_5$–CP–CA, $Fe_{85}Ce_{10}W_5$–CP–CA($NA_{1.0}$), and their precursors before being ignited are shown in Figure 4. As shown in Figure 4A,B, the precursor of $Fe_{85}Ce_{10}W_5$–CP–CA($NA_{1.0}$) shows stronger agglomeration than that of $Fe_{85}Ce_{10}W_5$–CP–CA, and the combustion of dried gel at the presence of nitrate contributes to the agglomeration of the particles, and results in poor pore connectivity of $Fe_{85}Ce_{10}W_5$–CP–CA($NA_{1.0}$), thus decreasing its pore volume. The particles in $Fe_{85}Ce_{10}W_5$–CP–CA have an outstanding distribution, contributing to the smaller pores and larger pore volume, which is beneficial to mass transfer and diffusion. Meanwhile, the diffusion of reactant gases and product gases among the pores of catalysts is important for NH_3–SCR reaction [31–33]. In addition, the removal of nitrate also decreases the particles' average diameter of $Fe_{85}Ce_{10}W_5$–CP–CA as calculated from the SEM in Figure 4C,D, which is in accordance with the particle sizes calculated according to the Scherrer equation.

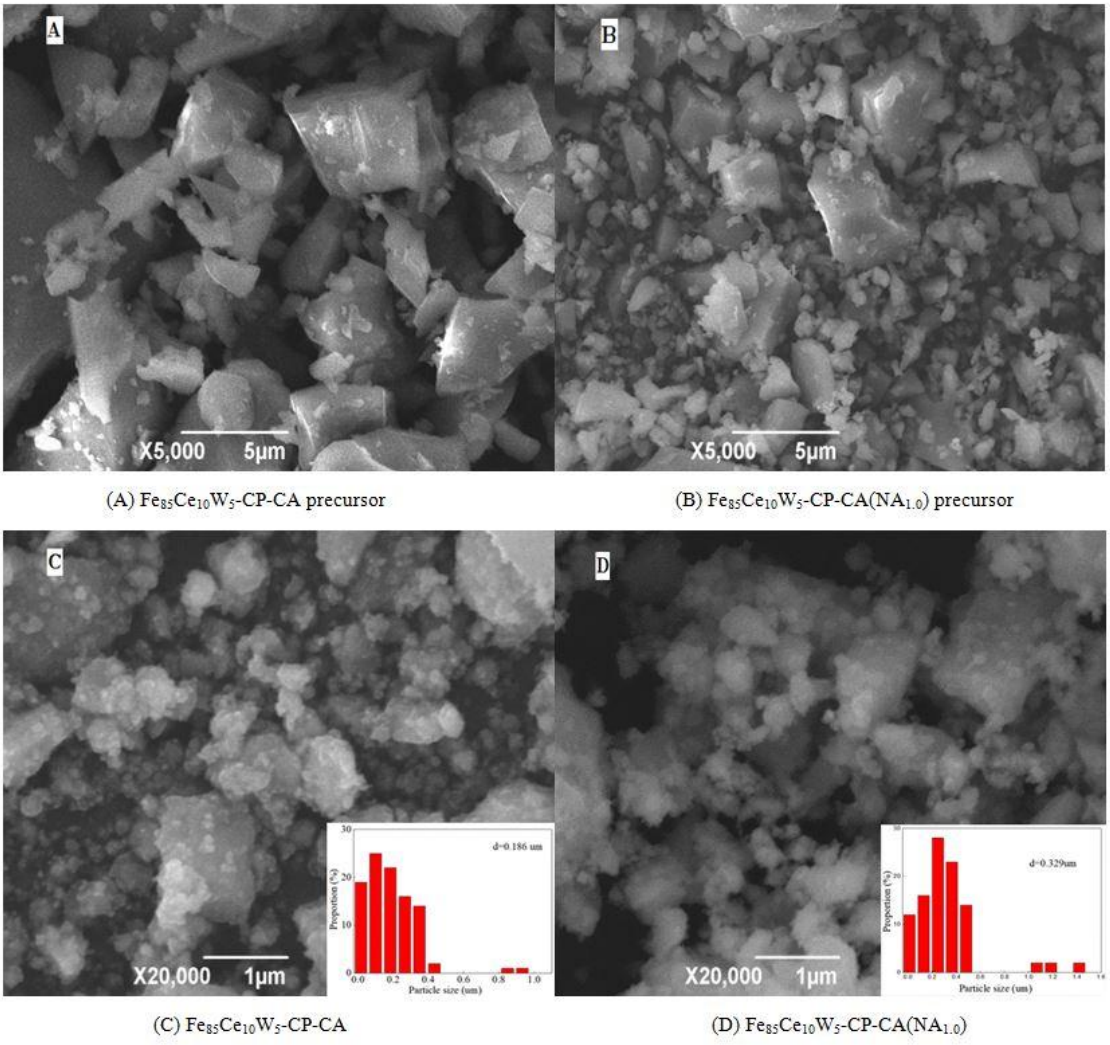

Figure 4. The scanning electron microscope (SEM) images of $Fe_{85}Ce_{10}W_5$–CP–CA and $Fe_{85}Ce_{10}W_5$–CP–CA(NA1.0) before and after calcination, respectively.(**A**) $Fe_{85}Ce_{10}W_5$–CP–CA before calcination, (**B**) $Fe_{85}Ce_{10}W_5$–CP–CA(NA1.0) before calcination, (**C**) $Fe_{85}Ce_{10}W_5$–CP–CA after calcination, (**D**) $Fe_{85}Ce_{10}W_5$–CP–CA(NA1.0) after calcination.

2.3.3. N_2 Adsorption–Desorption

The porosity and the pore size distribution of the as-prepared two catalysts were determined using N_2 adsorption–desorption. Figure 5 displays the N_2 adsorption–desorption isotherms, the pore size distributions of $Fe_{85}Ce_{10}W_5$–CP–CA and $Fe_{85}Ce_{10}W_5$–CP–CA($NA_{1.0}$), and their NO_x conversions over per surface area in one hour (mg/(m^2·h)). As can be observed, the isotherm of $Fe_{85}Ce_{10}W_5$–CP–CA(NA1.0) can be recognized as a type IV N2 adsorption/desorption isotherm according to the International Union of Pure and Applied Chemistry (IUPAC) classification, and it presents mainly meso-pores (2–50 nm), however, the hysteresis loops of Fe85Ce10W5–CP–CA(NA1.0) and Fe85Ce10W5–CP–CA are the H2 and H1 type [32,34], respectively. This demonstrates that the removal of nitrate promotes the formation of meso-pores in magnetic, and the Fe85Ce10W5–CP–CA catalyst shows uniform and regular meso-pores, which was confirmed by the results of the pore diameter distribution in Figure 5B [35]. Interesting, the Brunauer-Emmett and Teller (BET) surface area of $Fe_{85}Ce_{10}W_5$–CP–CA was 90.85 m^2/g, a little smaller than that of $Fe_{85}Ce_{10}W_5$–CP–CA($NA_{1.0}$) (93.13 m^2/g), as shown in Table 2. Usually, a large BET surface area is beneficial to enhance the catalytic ability of the catalyst. Thus, the NO_x conversions at low-temperature over per surface area of catalysts in one

hour were calculated, and it was found that $Fe_{85}Ce_{10}W_5$–CP–CA showed a higher NO_x conversion over per surface area in one hour than $Fe_{85}Ce_{10}W_5$–CP–CA($NA_{1.0}$) at 150~200 °C.

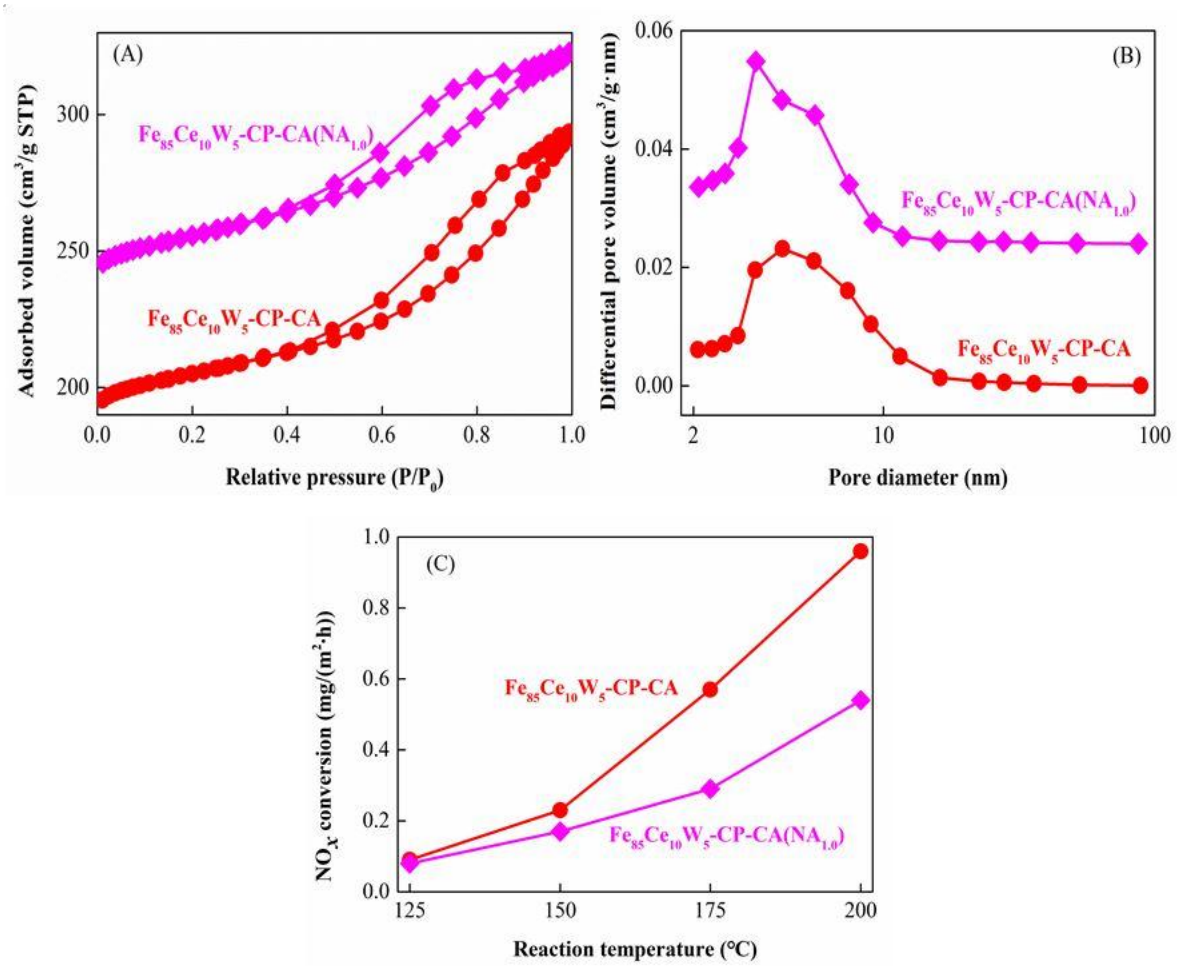

Figure 5. N_2 adsorption and desorption isotherms (**A**), pore diameter distributions (**B**), and desorption cumulative pore volume (**C**) of catalysts.

Table 2. The surface area, pore volume, diameter, and average crystallite size of the catalysts.

Samples	S_{BET} [a] (m^2/g)	Pore Volume [b] (cm^3/g)	Pore Diameter [c] (nm)	D [d] (nm)
$Fe_{85}Ce_{10}W_5$–CP–CA	90.850	0.178	6.170	13.000
$Fe_{85}Ce_{10}W_5$–CP–CA($NA_{1.0}$)	93.130	0.146	4.920	14.400

[a] Brunauer-Emmett and Teller (BET) surface area; [b] Barrett-Joyner and Halenda (BJH) desorption pore volume; [c] Barrett-Joyner and Halenda (BJH) desorption pore diameter; [d] Calculated according to the Scherrer equation.

2.3.4. X-ray Photoelectron Spectroscopy (XPS) and H_2-Temperature Program Reduction (H_2-TPR)

To investigate the influence of nitrate on the elements' concentrations and chemical states on the surface of the catalyst, the XPS spectra of $Fe_{85}Ce_{10}W_5$–CP–CA and $Fe_{85}Ce_{10}W_5$–CP–CA($NA_{1.0}$) were carried out. As can be noted from Table 3, the re-introduction of nitrate decreased the concentrations of cerium and tungsten on the surface of $Fe_{85}Ce_{10}W_5$–CP–CA, and increased its surface concentration of iron. Higher surface Ce concentration contributes to the excellent reduction ability, which is widely known to be conducive for NH_3–SCR reaction [36]. To further study the influence of nitrate on the redox properties of the magnetic Fe–Ce–W mixed oxides catalyst, the H_2–TPR curves of $Fe_{85}Ce_{10}W_5$–CP–CA and $Fe_{85}Ce_{10}W_5$–CP–CA($NA_{1.0}$) were obtained. The results in Figure 6 show that there exists one peak at the temperature range of 300~500 °C for these two samples, attributed to the reduction

from Fe_2O_3 to Fe_3O_4 at the range of 300~400 °C and the further reduction of Fe_3O_4 to FeO at about 500 °C [37–39]. Interesting, the re-introduction of nitrate enhanced the low-temperature reducibility of $Fe_{85}Ce_{10}W_5$–CP–CA by increasing its surface concentration of iron species, which is confirmed by the results of XPS in Figure 5. Meanwhile, the re-introduction of nitrate decreased the NH_3–SCR activity of the magnetic $Fe_{85}Ce_{10}W_5$–CP–CA catalyst.

Table 3. The X-ray photoelectron spectroscopy (XPS) results of catalysts.

Samples	Surface Atomic Concentrations (%)							
	Fe^{2+}	Fe^{3+}	Fe_{total}	Ce	W	O_α	O_β	O_{total}
$Fe_{85}Ce_{10}W_5$-CP-CA	5.65	11.71	17.36	7.24	2.89	15.82	56.69	72.51
$Fe_{85}Ce_{10}W_5$-CP-CA($NA_{1.0}$)	5.73	11.83	17.56	6.33	2.36	16.09	57.66	73.75

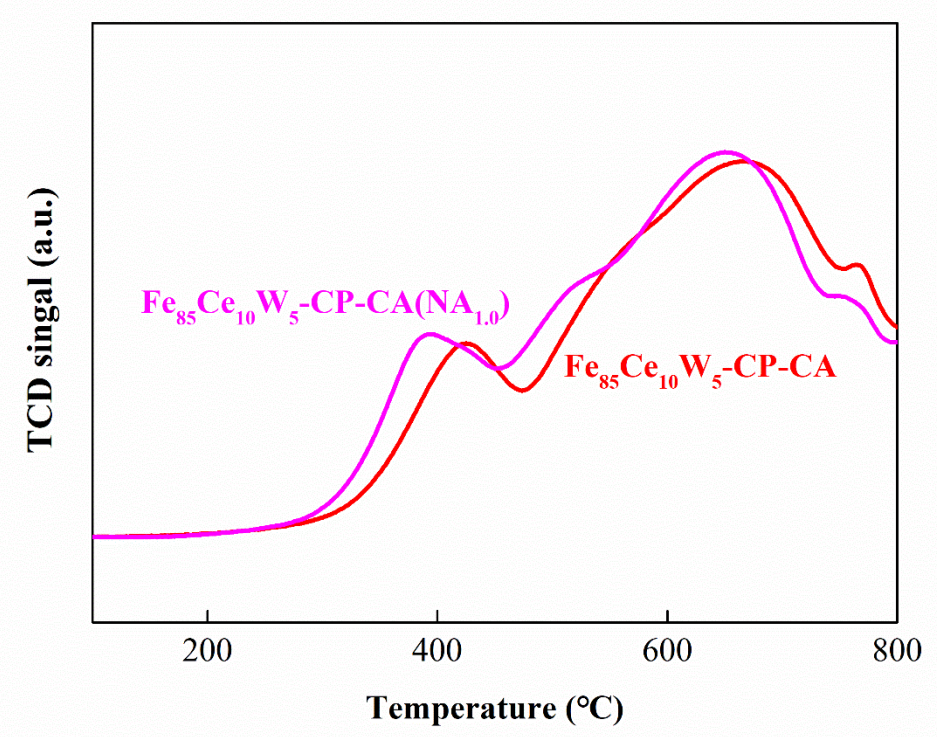

Figure 6. H_2-temperature program reduction (H_2-TPR) profiles of the catalysts.

2.3.5. NH_3–Temperature Programmed Desorption (NH_3-TPD)

The peak position of NH_3–TPD refers to the adsorption strength, and the peaks at 100~200, 200~350 and >350 °C are attributed to the weakly acidic site, the medium-strong acid site, and the strong acid site [40], respectively. From the results in Figure 7, it can be seen that there exists weak acid sites, medium acid site, and strong acid sites on the surface of the magnetic Fe–Ce–W mixed oxide catalysts. The NH_3 species adsorbed on the weak acid sites and the medium acid sites were mainly assigned to the coordinated NH_3 bound to Lewis acid sites and the partial ionic NH_4^+ bound to Brønsted acid sites [41–43]. The re-introduction of nitrate decreased the adsorption of NH_3 on the magnetic $Fe_{85}Ce_{10}W_5$–CP–CA catalyst, particularly decreasing the intensity of its weak and medium-strong acidic sites. Combined with the results of XRD and SEM, we speculate that the re-introduction of nitrate results in a severe agglomeration of amorphous iron and tungsten species of the magnetic $Fe_{85}Ce_{10}W_5$–CP–CA catalyst, and its acid center could be covered or decompose in this process, thereby decreasing the intensity of its weak and medium-strong acidic sites. Therefore, the re-introduction of nitrate modifies the surface structure of the magnetic $Fe_{85}Ce_{10}W_5$–CP–CA catalyst, and shows better

adsorption of the NH_3 reactants than $Fe_{85}Ce_{10}W_5$–CP–CA($NA_{1.0}$) at 125~250 °C, which is considered to be a key factor in improving the low-temperature NH_3–SCR activity of the catalyst.

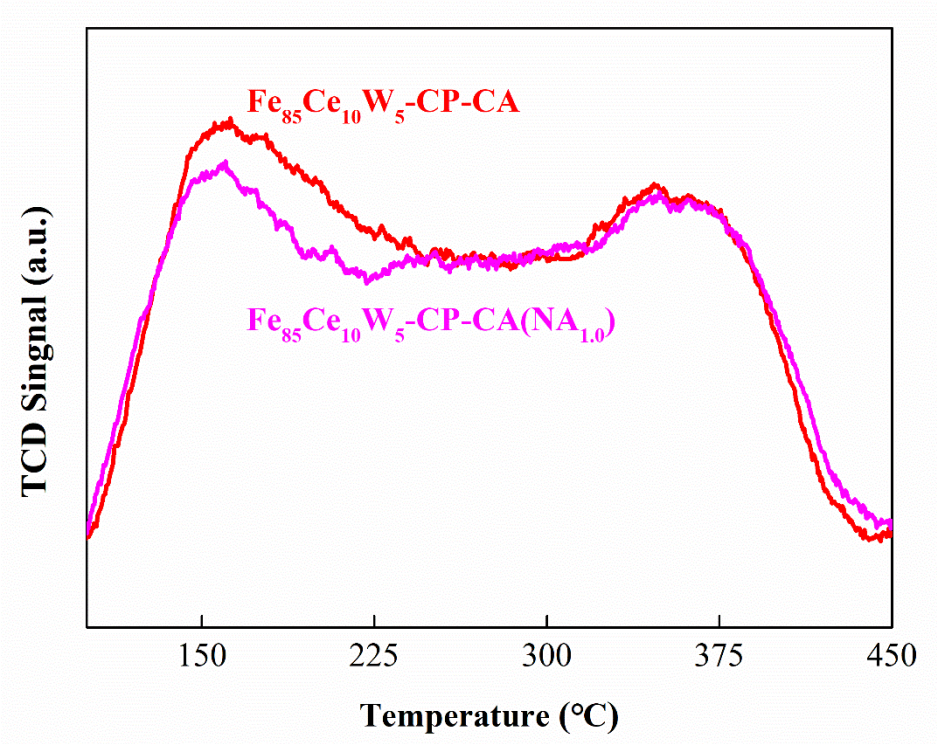

Figure 7. NH_3–temperature programmed desorption (NH_3-TPD) profiles of the catalysts.

2.4. Catalytic Mechanism

To identify the presence of the adsorbed NH_3 species in the SCR process on the surface of $Fe_{85}Ce_{10}W_5$–CP–CA, the in situ diffuse reflectance infrared Fourier transform spectroscopy (DRIFTS) spectra of three transient experiments were recorded under a steady-state condition, and the results are presented in Figure 8. As illustrated in Figure 8A, after NH_3 adsorption and N_2 purge at 250 °C, $Fe_{85}Ce_{10}W_5$–CP–CA showed several bands located at 1188, 1406, 1587, 3256, and 3351 cm^{-1}. The bands located at 1188 and 1587 cm^{-1} can be attributed to the coordinated NH_3 on the Lewis acid sites, and the band located at 1406 cm^{-1} can be ascribed to the ionic NH_4^+ bound to the Brønsted acid site, while the bands of 3256 and 3351 cm^{-1} corresponded to the N–H stretching modes of the coordinated NH_3 connected to the Lewis acid sites [27,44–48]. After the introduction of NO + O_2 for 10 s, the adsorption peaks of the coordinated NH_3 on the Lewis acid sites (located at 1188 and 1587 cm^{-1}) and the N–H stretching modes of coordinated NH_3 connected to the Lewis acid sites (located at 3256 and 3351 cm^{-1}) disappeared, and the intensity of ionic NH_4^+ bound to the Brønsted acid site at 1406 cm^{-1} also became weakened. At the same time, the bidentate nitrates (1002 and 1547 cm^{-1}), M–NO_2 formed by the reaction between M–OH and NO_x (1350 and 3639 cm^{-1}) and the bridging nitrate (1618 cm^{-1}) species appeared [44–47]. As shown in Figure 8B, after nitrogen oxide species adsorption and N_2 purge at 250 °C, $Fe_{85}Ce_{10}W_5$–CP–CA showed several bands ascribed to M–NO_2 formed by the reaction between M–OH and NO_x(1353 cm^{-1}), bidentate nitrates (1560 cm^{-1}), and bridging nitrate (1621 cm^{-1}), respectively [48–50]. After the introduction of NH_3 for 10 s, the intensity of adsorption peaks of M–NO_2 (1353 cm^{-1}) and bridging nitrate (1621 cm^{-1}) became weakened, and the band at 1560 cm^{-1} ascribed to the bidentate nitrates disappeared. The IR bands assigned to the coordinated NH_3 on the Lewis acid sites (1189 and 1587 cm^{-1}), the ionic NH_4^+ bound to the Brønsted acid site (1439 cm^{-1}), and the N–H stretching modes of the coordinated NH_3 connected to the Lewis acid sites (3255 and 3364 cm^{-1}) appeared [27,47–50]. Figure 8C shows the experimental results of the introduction of NH_3 + NO+O_2 gases over $Fe_{85}Ce_{10}W_5$–CP–CA at 250 °C. It can clearly be seen that the IR bands ascribed to

the coordinated NH_3, the N–H stretching modes of the coordinated NH_3 and the ionic NH_4^+ appeared, and their intensity gradually became stronger with the increase in the NH_3 + NO + O_2 introduction. However, the adsorption peaks at about 1350 and 1562 cm^{-1} ascribed to M–NO_2 and bidentate nitrate also appeared and then quickly vanished when NH_3 + NO + O_2 gases were introduced into the reaction tank. Therefore, it can be concluded that the reaction between the adsorbed NH_3 species with gaseous NO + O_2 or the adsorbed NO_x species might occur over $Fe_{85}Ce_{10}W_5$–CP–CA at 250 °C, obeyed both E–R and L–H mechanisms, and E–R was its main mechanism.

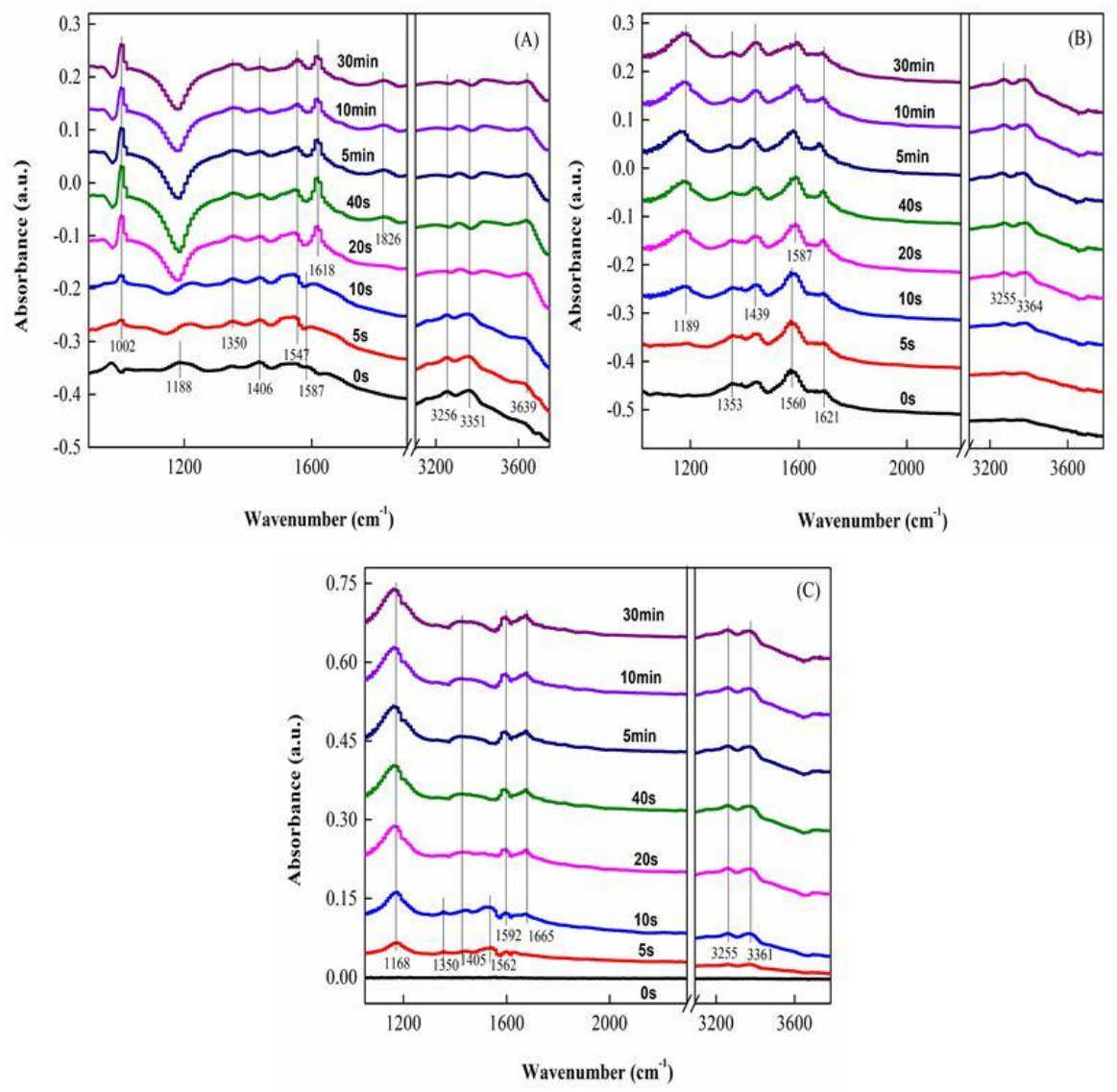

Figure 8. In situ diffuse reflectance infrared Fourier transform spectroscopy (DRIFTS) of Fe85Ce10W5–CP–CA catalyst under transient reactions at 250 °C. (**A**) Between nitrogen oxides and pre-adsorbed NH_3 species. (**B**) Between NH_3 and pre-adsorbed nitrogen oxides species. (**C**) The NH_3, NO, and O_2 species.

3. Experimental

3.1. Synthesis of the Catalyst

$Fe^{III}(NO_3)_3{\cdot}9H_2O$, $Ce^{III}(NO_3)_3{\cdot}6H_2O$, $(NH_4)_6H_2W^{VI}{}_{12}O_{40}{\cdot}nH_2O$, $NH_3{\cdot}H_2O$, and citric acid were used as the precursors, the precipitator, and the complexing agent, respectively. For

the preparation of magnetic iron–cerium–tungsten mixed oxide catalyst through the spread self-combustion of dried gel without nitrate, a certain amount of $Fe^{III}(NO_3)_3{\cdot}9H_2O$, $Ce^{III}(NO_3)_3{\cdot}6H_2O$, and $(NH_4)_6H_2W^{VI}{}_{12}O_{40}{\cdot}nH_2O$ were dissolved in the de-ionized water by keeping their molar ratio at 85:10:5. After magnetic stirring evenly, this solution was titrated into ammonia water of 2 mol/L until the pH value of 9–10. The obtained precipitation was fully washed by the de-ionized water to reduce the nitrate ion in it, and then a certain amount of citric acid was added into the washed precipitation with the molar ratio of citric acid/(Fe + Ce + W) as 1.0. After being stirred for 3 h under water bath at 50 °C, the citric acid dissolved solution were treated by microwave irradiation for 10 min with 36.4% power (microwave irradiation 8 s, 14 s suspended for a cycle with full power) using a household microwave oven (EG8MEA6-NR, 2.45 GHz, 800 W) to ignite, and this catalyst is denoted as $Fe_{85}Ce_{10}W_5$–CP–CA. The preparation of the catalyst by re-introducing nitric acid into the citric acid dissolved solution is similar to the preparation of $Fe_{85}Ce_{10}W_5$–CP–CA, which can be expected by adding a certain amount of nitric acid into the citric acid dissolved co-precipitation precursor before the water bath, which can be denoted as $Fe_{85}Ce_{10}W_5$–CP–CA (NA_x, x = 0.5, 1.0, 2.0), where x is the molar ratio of nitric acid/NO_3^- in both $Fe(NO_3)_3$ and $Ce(NO_3)_3$.

3.2. Catalytic Measurement and Characterization

The catalytic measurements of NO_x abatement with NH_3 were carried out in a one-dimensional transversely fixed quartz reactor. The simulated gas consisted of 1000 ppm NH_3, 1000 ppm NO, 3 vol.% O_2, and the balanced N_2 with the total flow of 2000 mL/min. The samples used in each experiment were 2 mL with a gas hourly space velocity (GHSV) of 60,000 h^{-1}. The concentrations of NO_x and O_2 were monitored via a flue gas analyzer (Model 60i, Thermo Fisher Scientific Co. Ltd., Waltham, MA, USA). NO_x conversion is defined by the following equation:

$$\text{NOx conversion } (\%) = \frac{\text{C(NOx) inlet} - \text{C(NOx) outlet}}{\text{C(NOx) inlet}} \quad (1)$$

The thermal decomposition properties of the precursor before being ignited were determined with a thermal gravimetric analyzer (Netzsch, Selb, Germany, STA449 F3) under an air atmosphere. The surface morphology of the catalyst was measured on a SEM (Japan, Shimadzu). In addition, the physicochemical properties of the samples were also characterized via XRD, N_2 adsorption–desorption, XPS, H_2–TPR, and NH_3–TPD as the same as our previous research [27]. The average crystallite sizes of γ-Fe_2O_3 in $Fe_{85}Ce_{10}W_5$–CP–CA and $Fe_{85}Ce_{10}W_5$–CP–CA($NA_{1.0}$) were calculated according to the Scherrer equation:

$$D = \frac{k\lambda}{\beta \cos(\theta)} \quad (2)$$

where k is the shape factor (k = 0.9); λ is the wavelength of radiations; and β is the FWHM (full width at half maxima). Finally, the NH_3–SCR mechanism over $Fe_{85}Ce_{10}W_5$–CP–CA at 250 °C was acquired by in situ diffuse reflection infrared Fourier transform spectroscopy (in situ DRIFTS).

4. Conclusions

The nitrate brought from metal nitrates could participate in the spread self-combustion of citric acid dried gel. The removal of nitrate contributes to optimize the structure properties and acid sites of the magnetic Fe–Ce–W mixed oxide catalyst. The removal of nitrate helps in the formation of dispersive gamma–Fe_2O_3 in $Fe_{85}Ce_{10}W_5$–CP–CA, accelerating the crystallite rate and refining the particle size, and it shows a wider pore size distribution than $Fe_{85}Ce_{10}W_5$–CP–CA($NA_{1.0}$). At the same time, the removal of nitrate also enhances the concentrations of cerium/tungsten on the surface of the magnetic catalyst and its low-temperature adsorption of NH_3. Therefore, the re-introduction of nitrate decreases the low-temperature NH_3–SCR activity of $Fe_{85}Ce_{10}W_5$–CP–CA, and both E–R and L–H mechanisms exist over $Fe_{85}Ce_{10}W_5$–CP–CA at 250 °C.

Author Contributions: Formal analysis, S.-m.W.; Investigation, B.Y.; Resources, W.L.; Writing-original draft, X.N.; Writing-review & editing, Z.-b.X. All authors have read and agreed to the published version of the manuscript.

Funding: This research was funded by Bin Yang grant number No. 2016YFB0600601, Zhi-bo Xiong grant number No. 51406118 and Wei Lu grant number No. QD2015017. And The APC was funded by Bin Yang.

Acknowledgments: This work was supported by the National Key Research and Development Program of China (No. 2016YFB0600601), the National Science Foundation of China (No. 51406118), and the Program of Special Appointment (Eastern Scholar) at the Shanghai Institutions of Higher Learning (No. QD2015017).

Conflicts of Interest: The authors declare no conflicts of interest.

References

1. Parvulescu, V.; Delmon, B.; Grange, P. Catalytic removal of NO. *Catal. Today* **1998**, *46*, 233–316. [CrossRef]
2. Forzatti, P.; Nova, I.; Tronconi, E. Enhanced NH3 selective catalytic reduction for NO_x abatement. *Angew. Chem. Int. Edit.* **2009**, *48*, 8366–8368. [CrossRef] [PubMed]
3. Husain, D. Chemistry of atmospheres: An introduction to the chemistry of atmospheres of earth the planets and their satellites by R. P. *Wayne. J. Photo. Chem. Photobiol. A Chem.* **1992**, *63*, 253–254. [CrossRef]
4. Zhao, S.J.; Wang, L.; Wang, Y.; Li, X. Hierarchically porous $LaFeO_3$ perovskite prepared from the pomelo peel bio-template for catalytic oxidation of NO. *J. Phys. Chem. Solids* **2018**, *116*, 43–49. [CrossRef]
5. Amanatidis, S.; Ntziachristos, L.; Giechaskiel, B.; Bergmann, A.; Samaras, Z. Impact of selective catalytic reduction on exhaust particle formation over excess ammonia events. *Environ. Sci. Technol.* **2014**, *48*, 11527–11534. [CrossRef]
6. Gu, Q.; Wang, L.; Wang, Y.; Li, X. Effect of praseodymium substitution on $La_{1-x}Pr_xMnO_3$ (x=0-0.4) perovskites and catalytic activity for NO oxidation. *J. Phys. Chem. Solids* **2019**, *133*, 52–58. [CrossRef]
7. Ning, P.; Song, Z.X.; Li, H.; Zhang, Q.L.; Liu, X.; Zhang, J.H.; Tang, X.S.; Huang, Z.Z. Selective catalytic reduction of NO with NH_3 over CeO_2-ZrO_2-WO_3 catalysts prepared by different methods. *Appl. Surf. Sci.* **2015**, *332*, 130–137. [CrossRef]
8. Shang, D.H.; Zhong, Q.; Cai, W. High performance of NO oxidation over Ce-Co-Ti catalyst: The interaction between Ce and Co. *Appl. Surf. Sci.* **2015**, *325*, 211–216. [CrossRef]
9. Dunn, J.P.; Koppula, P.R.; Stenger, H.G.; Wachs, I.E. Oxidation of sulfur dioxide to sulfur trioxide over supported vanadia catalysts. *Appl. Catal. B* **1998**, *19*, 103–117. [CrossRef]
10. Boningari, T.; Ettireddy, P.R.; Somogyvari, A.; Liu, Y.; Vorontsov, A.; McDonald, C.A.; Smirniotis, P.G. Influence of elevated surface texture hydrated titania on Ce-doped Mn/TiO_2 catalysts for the low-temperature SCR of NO_x under oxygen-rich conditions. *J. Catal.* **2015**, *325*, 145–155. [CrossRef]
11. Narasimharao, K.; Malik, M.A.; Mokhtar, M.M.; Basahel, S.N.; Al-Thabaiti, S.A. Iron oxide supported sulfated TiO_2 nanotube catalysts for NO reduction with propane. *Ceram. Int.* **2014**, *40*, 4039–4053. [CrossRef]
12. Jiang, Y.; Gao, X.; Zhang, Y.X.; Wu, W.H.; Song, H.; Luo, Z.Y.; Cen, K.F. Effects of $PbCl_2$ on selective catalytic reduction of NO with NH_3 over vanadia-based catalysts. *J. Hazard. Mater.* **2014**, *274*, 270–278. [CrossRef] [PubMed]
13. Kröcher, O.; Elsener, M. Chemical deactivation of V_2O_5-WO_3/TiO_2 SCR catalysts by additives and impurities from fuels, lubrication oils, and urea solution: I. catalytic studies. *Appl. Catal. B* **2008**, *77*, 215–227. [CrossRef]
14. Li, X.D.; Wang, C.; Huang, J.Q.; Yuan, Y.; Wang, B.; Zhang, H.B.; Xia, F.; Xiao, J.Z. The effects of Cu-content on $Mg_2Cu_xFe_1O_{3.5+x}$ electrodes for YSZ-based mixed-potential type NH_3 sensors. *Ceram. Int.* **2016**, *42*, 9363–9370. [CrossRef]
15. Balle, P.; Geiger, B.; Kureti, S. Selective catalytic reduction of NOx by NH3 on Fe/HBEA zeolite catalysts in oxygen-rich exhaust. *Appl. Catal. B* **2009**, *85*, 109–119. [CrossRef]
16. Duan, L.B.; Duan, Y.; Sarbassov, Y.; Li, Y.; Anthony, E. SO_3 formation under oxy-CFB combustion conditions. *Int. J. Greenh. Gas Con.* **2015**, *43*, 172–178. [CrossRef]
17. Zhao, S.J.; Wang, Y.; Wang, L.; Jin, Y.L. Preparation, characterization and catalytic application of hierarchically porous $LaFeO_3$ from a pomelo peel template Inorg. *Chem. Front.* **2017**, *4*, 994–1002.
18. Chen, J.; Duan, L.; Donat, F.; Müller, C.; Anthony, E.; Fan, M. Self-activated nanostructured composite for improved CaL-CLC technology. *Chem. Eng. J.* **2018**, *351*, 1038–1046. [CrossRef]
19. Kazantsev, P.A.R.V.; Pankina, G.V.; Maslakov, K.I.; Lunin, B.S.; Eliseev, O.L. Carbon-Silica composite as an effective support for iron fischer-tropsch synthesis catalysts. *Energy Technol.* **2019**, *7*, 1800961.

20. Chen, J.; Duan, L.; Sun, Z. Accurate control of cage-Like CaO hollow microspheres for enhanced CO_2 capture in calcium looping via a template-assisted synthesis approach. *Environ. Sci. Technol.* **2019**, *53*, 2249–2259. [CrossRef]
21. Wu, D.; Shi, Z.F.; Zhang, X.P.; Wu, X.H. Progress of studies on preparation of TiO_2 photocatalysts with sol-gel auto igniting synthesis. *Earth Environ. Sci.* **2017**, *94*, 1–4. [CrossRef]
22. Parida, K.M.; Reddy, K.H.; Martha, S.; Das, N.; Bisawal, N. Fabrication of nanocrystalline $LaFeO_3$: An efficient sol–gel auto-combustion assisted visible light responsive photocatalyst for water decomposition. *Int. J. Hydrogen Energy* **2010**, *35*, 12161–12168. [CrossRef]
23. Sijo, A.K. Magnetic and structural properties of $CoCr_xFe_{2-x}O_4$ spinels prepared by solution self-combustion method. *Ceram. Int.* **2017**, *43*, 2288–2290. [CrossRef]
24. Cannas, C.; Musinu, A.; Peddis, D.; Piccaluga, G. New synthesis of ferrite-silica nanocomposites by a sol-gel auto-combustion. *J. Nanopart. Res.* **2004**, *6*, 223–232. [CrossRef]
25. Kaitlyn, A.; George, K.S. Synthesis of GAGG: Ce3+ powder for ceramics using mechanochemical and solution combustion methods. *J. Am. Ceram. Soc.* **2018**, *101*, 3837–3849.
26. Yeh, C.L.; Ke, C.Y. Synthesis of TiB_2-Al_2O_3-FeAl composites via self-sustaining combustion with Fe_2O_3/TiO_2-based thermite mixtures. *Ceram. Int.* **2018**, *44*, 16030–16034. [CrossRef]
27. Xiong, Z.B.; Ning, X.; Zhou, F.; Yang, B.; Tu, Y.W.; Jin, J.; Lu, W.; Liu, Z.H. Environment-friendly magnetic Fe-Ce-W catalyst for the selective catalytic reduction of NO_x with NH_3: Influence of citric acid content on its activity-structure relationship. *RSC Adv.* **2018**, *8*, 21915–21925. [CrossRef]
28. Ianoş, R.; Tăculescu, A.; Păcurariu, C.; Lazău, I. Solution combustion synthesis and characterization of magnetite, Fe_3O_4, nanopowders. *J. Am. Ceram. Soc.* **2012**, *95*, 2236–2240. [CrossRef]
29. Ianoş, R.; Moacă, E.A.; Căpraru, A.; Lazău, R.; Păcurariu, C. Maghemite, γ-Fe_2O_3, nanoparticles preparation via carbon-templated solution combustion synthesis. *Ceram. Int.* **2018**, *44*, 14090–14094. [CrossRef]
30. Zhao, J.; Liang, Y.; Yan, H.; Gu, A.; He, S.; Liu, J. Preparation of nano-MnZn ferrite by gel-self-combustion technique. *J. Mater. Sci. Eng.* **2003**, *21*, 68–71.
31. Xu, L.T.; Niu, S.L.; Lu, C.M.; Zhang, Q. Influence of calcination temperature on $Fe_{0.8}Mg_{0.2}O_z$ catalyst for selective catalytic reduction of NO_x with NH_3. *Fuel* **2018**, *219*, 248–258. [CrossRef]
32. Zhao, K.; Meng, J.P.; Lu, J.Y.; He, Y.; Huang, H.Z.; Tang, Z.C.; Zhen, X.P. Sol-gel one-pot synthesis of efficient and environmentally friendly iron-based catalysts for NH_3-SCR. *Appl. Surf. Sci.* **2018**, *445*, 454–461. [CrossRef]
33. Zhang, Q.L.; Liu, X.; Ning, P.; Song, Z.X. Enhanced performance in NO_x reduction by NH_3 over a mesoporous Ce-Ti-MoOx catalyst stabilized by a carbon template. *Catal. Sci. Technol.* **2015**, *5*, 2260–2269. [CrossRef]
34. Liu, F.D.; He, H. Structure-activity relationship of iron titanate catalysts in the selective catalytic reduction of NO_x with NH_3. *J. Phys. Chem. C* **2010**, *114*, 16929–16936. [CrossRef]
35. Wang, R.N.; Wu, X.; Zou, C.L.; Li, X.J.; Du, Y.L. NO_x removal by selective catalytic reduction with ammonia over a hydrotalcite-derived NiFe mixed oxide. *Catalysts* **2018**, *8*, 384. [CrossRef]
36. Tan, J.B.; Wei, Y.C.; Sun, Y.Q.; Liu, J.; Zhao, Z.; Song, W.Y.; Li, J.M.; Zhang, X. Simultaneous removal of NO_x and soot particulates from diesel engine exhaust by 3DOM Fe-Mn oxide catalysts. *J. Ind. Eng. Chem.* **2018**, *63*, 84–94. [CrossRef]
37. Wang, H.; Ning, P.; Zhang, Q.; Liu, X.; Zhang, T.; Fan, J.; Wang, J.; Long, K. Promotional mechanism of WO_3 over RuO_2-Fe_2O_3 catalyst for NH_3-SCO reaction. *Appl. Catal. A* **2018**, *561*, 158–167. [CrossRef]
38. Wang, H.; Qu, Z.P.; Xie, H.B.; Maeda, N.; Lei, M.; Wang, Z. Insight into the mesoporous $Fe_xCe_{1-x}O_{2-\delta}$ catalysts for selective catalytic reduction of NO with NH_3: Regulable structure and activity. *J. Catal.* **2016**, *338*, 56–67. [CrossRef]
39. Abolfazl, B.R.; Rezaei, M. Low temperature CO oxidation over Fe-Co mixed oxide nanocatalysts. *Chem. Eng. J.* **2012**, *184*, 141–146.
40. Li, X.S.; Li, K.; Yue, Z.P.; Li, X.Y.N.; Zhang, D.; Wang, J.J.; Chen, J.; Li, H. Interaction of phosphorus with a $FeTiO_x$ catalyst for selective catalytic reduction of NO_x with NH_3: Influence on surface acidity and SCR mechanism. *Chem. Eng. J.* **2018**, *347*, 173–183. [CrossRef]
41. Xiong, Z.B.; Liu, J.; Zhou, F.; Liu, D.Y.; Lu, W.; Jin, J.; Ding, S.F. Selective catalytic reduction of NO_x with NH_3 over iron-cerium-tungsten mixed oxide catalyst prepared by different methods. *Appl. Surf. Sci.* **2017**, *406*, 218–225. [CrossRef]

42. Xiong, Z.B.; Bai, P.; Zhou, F.; Wu, C.; Lu, W.; Jin, J.; Ding, S.F. Magnetic iron-cerium-tungsten mixed oxide pellets prepared through critic acid sol-gel process assisted by microwave irradiation for selective catalytic reduction of NO_x with NH_3. *Powder Technol.* **2017**, *319*, 19–25. [CrossRef]
43. Li, X.; Li, J.H.; Yue, P.; Xu, B. Selective catalytic reduction of NO with NH_3 over novel iron-tungsten mixed oxide catalyst in a broad temperature range. *Catal. Sci. Technol.* **2015**, *5*, 4556–4564. [CrossRef]
44. Zhang, G.; Ren, J.J.; Liu, B.L.; Tian, M.; Zhou, H.W.; Zhao, J.S. In situ hydrothermal preparation and photocatalytic desulfurization performance of metallophthalocyanine sensitized SnO_2. *J. Inorg. Chim. Acta* **2018**, *471*, 782–787. [CrossRef]
45. Liu, Y.; Gu, T.T.; Weng, X.L.; Wang, Y. DRIFT studies on the selectivity promotion mechanism of Ca-modified Ce-Mn/TiO_2 catalysts for low-temperature NO reduction with NH_3. *J. Phys. Chem. A* **2012**, *116*, 16582–16592. [CrossRef]
46. Chen, P.; Tao, L.; Zhu, J.; Zhao, G.; Liu, Y.; Lu, Y. Morphology-controllable hexagonal-phase indium oxide in situ structured onto a thin-felt Al_2O_3/Al-fiber for the hydrogenation of CO_2 to methanol. *Energy Technol.* **2019**, *7*, 1800747. [CrossRef]
47. Liu, J.; Xiong, Z.B.; Zhou, F.; Lu, W.; Jin, J.; Ding, S.F. Promotional effect of H_2O_2 modification on the cerium-tungsten-titanium mixed oxide catalyst for selective catalytic reduction of NO with NH_3. *J. Phys. Chem. Solids* **2018**, *121*, 360–366. [CrossRef]
48. Castellanos, I.; Marie, O. An operando FT-IR study of the NO_x SCR over Co-HFER and Fe-HFER using acetylene as a reducing agent. *Catal. Today* **2017**, *283*, 54–65. [CrossRef]
49. Shi, J.; Zhang, Y.; Zhang, Z.H.; Fan, Z.Y.; Chen, M.X.; Zhang, Z.X.; Shangguan, W.F. Water promotion mechanism on the NH_3-SCR over Fe-BEA catalyst. *Catal. Commun.* **2018**, *115*, 59–63. [CrossRef]
50. Devadas, M.; KroCher, O.; Elsener, M.; Wokaun, A.; Mitrikas, G.; Söger, N.; Pfeifer, M.; Demel, Y.; Mussmann, L. Characterization and catalytic investigation of Fe-ZSM5 for urea-SCR. *Catal. Today* **2007**, *119*, 137–144. [CrossRef]